Mechanical Modulation of Ovarian Cancer Tumor Nodules under Flow

Christina Conrad, Kaitlin Moore, William J. Polacheck, Imran Rizvi*, and Giuliano Scarcelli*

Abstract*— *Objective: **Perfusion models are valuable tools to mimic complex features of the tumor microenvironment and to study cell behavior. In ovarian cancer, mimicking disease pathology of ascites has been achieved by seeding tumor nodules on a basement membrane and subjecting them to long-term continuous flow. In this scenario it is particularly important to study the role of mechanical stress on cancer progression. Mechanical cues are already known to be important in key cancer processes such as survival, proliferation, and migration. However, probing cell mechanical properties within microfluidic platforms has not been achievable with current technologies since samples are not easily accessible within most microfluidic channels.** ***Methods:*** **Here, to analyze the mechanical properties of cells within a perfusion chamber, we use Brillouin confocal microscopy, an all-optical technique that requires no contact or perturbation to the sample.** ***Results:*** **Our results indicate that ovarian cancer nodules under long-term continuous flow have a significantly lower longitudinal modulus compared to nodules maintained in a static condition.** ***Conclusion:*** **We further dissect the role of distinct mechanical perturbations (e.g. shear flow, osmolality) on tumor nodule properties.** ***Significance:*** **In summary, the unique combination of a long-term microfluidic culture and noninvasive mechanical analysis technique provides insights on the effects of physical forces in ovarian cancer pathology.**

***Index Terms*—Brillouin microscopy, mechanical properties, ovarian cancer, shear flow**

I. INTRODUCTION

A major cause of disease progression in patients with ovarian cancer is the accumulation of ascitic fluid within the abdomen [1]. Approximately 89% of patients with stage III or IV ovarian cancer develop ascites [2], [3]. The cause of fluid retention is not well-established and thought in-part to be due to lymphatic obstruction [3]–[5]. Palliative care such as paracentesis via percutaneous drainage or catheter drainage is frequently used to reduce ascites; however, symptoms can reappear in as little as 10 days [6]–[8]. Not only does fluid accumulation raise intra-abdominal pressure [9] and cause discomfort to the patient, but ascites facilitates cell phenotypic modulations and intervenes with treatment success. The clinical presence of ascites is indicative of increased transcoelomic metastasis [9], resistance to chemotherapy [3], and upregulated markers associated with poor prognosis, such as vascular endothelial growth factor (VEGF) [4], [7], [10].

While increasing evidence supports the role of ascites as a negative prognostic indicator in advanced-stage ovarian cancer, the impact of mechanical stress (*i.e.* flow-induced shear stress) on aggressiveness, and poor sensitivity to treatment, in ovarian cancer remains understudied. Recent studies [11, 12] demonstrated an increase in epithelial to mesenchymal transition (EMT), marked by changes such as increased spindle-like morphology, loss of E-cadherin, and upregulated vimentin, in 3D OVCAR5 tumors grown under continuous flow for 7 days [11], compared to equivalent static cultures. A concomitant flow-induced increase in expression and activation of the epidermal growth factor receptor [EGFR] was observed. Elevated EGFR signaling activity is understood to promote proliferation, invasiveness, and cell survival [12]. The experimental parameters used in this study informed the conditions used in the present study.

More recently. Nath *et al.* [12] demonstrated that flow-induced shear stress conferred resistance to carboplatin, compared to equivalent static cultures, despite higher drug uptake under flow [12]. This flow-induced resistance to carboplatin was associated with increased signaling of mitogen-activated protein kinase/extracellular signal-regulated kinase (MEK) and phosphorylated extracellular signal-regulated kinase (p-ERK). A variety of receptor tyrosine kinase (RTK) networks regulate MEK/ERK signaling, including the EGFR, which was confirmed to be upregulated under flow [12]. Interestingly, low-dose anti-EGFR photoimmunotherapy (PIT) resulted in comparable cytotoxic response in static and flow cultures, suggesting a role for targeted photochemistry-based therapies as part of rationally-designed combinations [12].

Ip *et al.* [1] used the human ovarian carcinoma SKOV-3 cell line formed into spheroids and embedded them on a 2-hydroxyethylmethacrylate (poly-HEMA) coated glass slide. Exposing tumors to both 0.002 dyne/cm^2 and 0.02 dyne/cm^2 for 24 hours induced gene expressions corresponding to EMT characterized by increased Snail, Slug, and N-cadherin, with decreased E-cadherin. Upregulated stem cell marker gene expressions were also observed including octamer-binding transcription factor 4 (Oct-4), c-Kit (CD117), ATP-binding

This work is supported by NC Translational and Clinical Sciences Institute (NCTraCS), supported by the National Center for Advancing Translational Sciences (NCATS), National Institutes of Health (R33CA204582, U01CA202177, UL1TR002489, R00CA175292); National Science Foundation (CMMI- 1929412), UNC-NCSU Joint BME Department Start-up Fund (WJP) and UNC-NCSU Joint BME Department Start-up Fund (IR).

C. Conrad and G. Scarcelli (Corresponding author email: scarc@umd.edu) are with the Fischell Department of Bioengineering, University of Maryland, College Park, MD 20742.

K. Moore is with the Wellman Center for Photomedicine, Massachusetts General Hospital and Harvard Medical School, Boston, MA 02114.

W.J. Polacheck and I. Rizvi are with the Joint Department of Biomedical Engineering, University of North Carolina at Chapel Hill and North Carolina State University, Chapel Hill, NC 27599 and Lineberger Comprehensive Cancer Center, University of North Carolina School of Medicine Chapel Hill, NC 27599. * denotes equal contribution

cassette G2 (ABCG2) and P-glycoprotein (P-gp) [1]. Moreover, flow increased chemoresistance after treatment of cisplatin (25 μM) or paclitaxel (100 nM) [1].

While molecular consequences under flow are partially established, there remains inadequate information on how exposure to physical stress modulates mechanical properties. Mechanical properties of cells and tissues are known to play a critical role in cancer behaviors such as migration, survival, and proliferation [13]–[15]. In ovarian cancer particularly, prior studies indicate ovarian cancer cells have a lower Young's modulus in contrast to benign cells, suggesting they are more susceptible to physical change under longitudinal forces; however, the exact mechanisms causing this behavior is not clear [16]–[20]. As flow confers a physical stress and has been shown to induce elongated morphology [21], we expected that mechanical properties (*i.e.* stiffness) would be modulated under flow compared to static conditions.

A limitation to standard mechanical analysis techniques is the need for contact with the sample, therefore making analysis of nodules embedded within a perfusion device impossible. To solve this issue, we apply Brillouin confocal microscopy, an all-optical approach based on an interaction between incident photons and thermally excited acoustic phonons within a material [22]. The Brillouin frequency shift describes the inelastic scattering of photons which can be related to the longitudinal modulus at high frequency. A high Brillouin shift indicates a rigid material, while liquid-like medium such as cytosol will result in a lower shift [23]. As biological samples exhibit frequency dependent behaviors and are nearly incompressible, the Brillouin-derived longitudinal modulus probes different properties from traditional stress-strain tests [24]. However, correlative studies demonstrate that a log-log linear relationship exists between the Brillouin longitudinal modulus and Young's modulus in biological tissues and cells [24]–[26]. Specifically, we recently demonstrated matching trends of the Young's modulus derived using AFM and the Brillouin-derived moduli in tumor nodules, thus validating the use of Brillouin microscopy for mechanical evaluation in these samples [27].

As previously mentioned, in the work presented here, we used the same perfusion platform, flow rates, and seeding densities described by Rizvi *et al.* [11], where a range of seeding densities and flow rates were evaluated. The conditions that resulted in consistent tumor growth and modulation of biological parameters over a 7-day timeframe (potentially mimicking physiologically-relevant conditions that are permissive to tumor growth), were then selected [11]. The shear stress conferred by the selected flow rate (~3 dyne/cm^2) is based on evidence that peritoneal shear stresses are in the range of 0.14 dyne/cm^2 to 11 dyne/cm^2 [28]. In the present study, the mechanical properties of 3D tumor nodules were characterized on day 7, and it was found the Brillouin shift was significantly lower under flow, compared to nodules in a static condition. To explain these differences, we considered that beyond shear stress, tumors in flow were exposed to cumulatively lower osmolality and higher nutrients compared to the static condition, where medium was replenished on days 3 and 6. The role of osmolality on mechanics was evaluated by measuring the Brillouin shift of static nodules with varied frequency of medium changes. Our results demonstrate a strong association between the extracellular fluid osmolality and the Brillouin shift of nodules. However, the cumulative history of osmolality did not influence the Brillouin shift, implying that osmotic differences between flow and static conditions were likely short-lived compared to the mechanical effects conferred by shear stress. We also examined the role of nutrients by changing fetal bovine serum concentrations and found effects on tumor growth but no differences in the Brillouin shift. Our findings of a decrease in tumor nodule stiffness under flow constitute an important question pertaining to the role of mechanical properties in ovarian cancer progression.

II. EXPERIMENTAL METHODS

A. Cell Culture

Epithelial ovarian cancer cells (NIH: OVCAR5) were grown in standard culture medium containing RPMI 1640 Medium (Gibco®, #11835030) no phenol red, 10% Fetal Bovine Serum (FBS), and 1% Penicillin-Streptomycin. For low nutrient experiments, the FBS percentage was reduced to 1% or 0.1%. Static Tumor Nodules: Corning® Matrigel® (Growth Factor Reduced (GFR) Basement Membrane Matrix Phenol Red-Free, *LDEV-Free #356231) was prepared by thawing overnight on ice at 4 °C. The following day, 250 μL of Matrigel was pipetted into wells of a pre-chilled sterile glass bottom 24-well plate (Greiner bio-one Sensoplate, #662892). Basement membranes were incubated at 37 °C for 20-30 minutes for gelation. Meanwhile, OVCAR5 cells were resuspended in medium with a concentration of 10^4 cells/mL and 1 mL was added per well. To replenish cell medium in the cultures, a 1 mL pipette was angled on the side of the well and medium was slowly aspirated and refilled. For flow vs. static experiments, cell medium was replenished on days 3 and 6. For medium change frequency experiments, nodules were exposed to either no change in medium for 7 days, change day on day 3/6, or a daily change of medium for 7 days. Osmolality: 20 μl of medium within each well was extracted and osmolality was measured using an Advanced® Micro-Osmometer Model 3300. Nodule Size: ImageJ was used to obtain the nodule area using an in-house developed macro [29]. Images were imported and 'find edges', 'make binary', and 'analyze particles' commands were successively performed.

B. Perfusion Chamber

The assembly of this device is previously described in literature [27]. Briefly, a double-sided adhesive (DSA) film (ARcare 90485; Adhesives Research) designed with 3 channels was pressed onto a glass cover slip. 20 μl of Matrigel was pipetted evenly into the channels of the DSA/glass coverslip assembly. The top sticky side of the DSA was removed and a polymethyl methacrylate (PMMA) part was placed on top. The DSA/PMMA construct was held together using screws. 100 cm tubing was inserted into the three inlet holes using an epoxy resin and hardener. In the same manner, 40 cm tubing was connected to the outlet. Cells were loaded into a 1 mL syringe at a concentration of $1*10^6$ cells/mL and loaded into a syringe pump (Harvard Apparatus, Pump 11 Pico Plus #170-2213). The selected concentration was previously established to enable matching cell adherence densities with the static condition [11]. The syringe was connected to the tubing using an 18-G blunt

needle and run at a flow rate of 100µl/min for 5 minutes to introduce cells into tube. The 1mL syringe was removed as cells reached the inlet of the microfluidic chip. A second syringe of 20 ml was filled with medium supplemented with 2% Matrigel and attached to the syringe pump. The pump was run at a flow rate of 100 µl/min to introduce cells/medium from tube to chip for 5 minutes. Finally, the pump was run at a flow rate of 2 µl/min for 7 days and the syringe of 2% Matrigel medium was replaced as needed. The microfluidic chip assembly was stored at 37 °C. A schematic of the microfluidic chip is shown in **Fig. 1**.

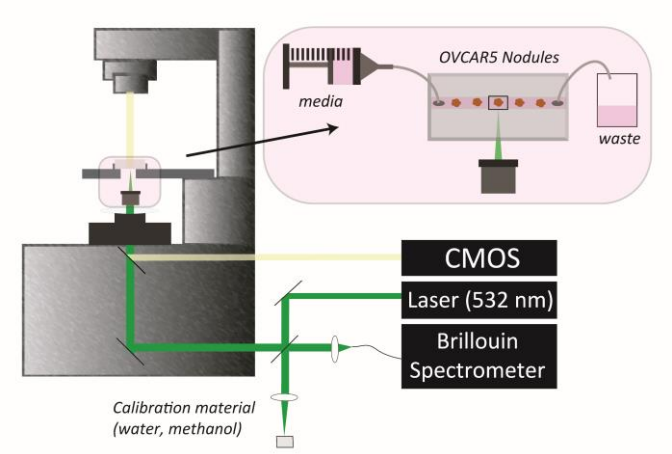

Fig. 1. Schematic of the set-up integrating Brillouin confocal microscopy with a perfusion chamber for the growth of adherent ovarian cancer nodules under flow.

C. Brillouin Confocal Microscopy

Brillouin light scattering is based on the interaction between light and the vibrational motion of molecules inside a material (acoustic phonons). Here, we used a single longitudinal mode laser (Torus 532 or Torus 660, Laser Quantum) with a wavelength of either 660 nm or 532 nm. Measurements comparing flow and static conditions were acquired in a previous set-up which utilized a 532 nm laser. To offer minimal absorption-mediated damage to samples, we now utilize a 660 nm light source [30].

The configuration of Brillouin used here has been previously described [27]. The laser was directed into the side port of an inverted microscope (Olympus, IX81) where light was focused through an objective lens into the sample. Backwards scattered light was then collected by the same objective lens and coupled into the Brillouin spectrometer. The Brillouin spectrometer is comprised of a two stage virtually imaged phased array (VIPA) in a cross-axis configuration [22]. Calibration was performed prior to the measurements using water (7.46 at 532 nm and 6.01 GHz at 660 nm) and methanol (6.48 at 532 nm and 5.22 GHz at 660 nm) which was further used to calculate the free spectral range (FSR) and convert the image in pixels to a frequency (GHz per pixel). Using a post-processing algorithm developed in MATLAB, the Brillouin spectrums were fit to a Lorentzian function and the Brillouin shift was obtained. To quantify average Brillouin shifts per nodule, a threshold was used to remove the values corresponding to the surrounding medium of the Brillouin maps and the remaining pixels were averaged. Brillouin maps were acquired in the XZ plane using a 60X/0.7 NA objective lens which has an approximate spatial resolution of 1 µm and axial resolution of 2 µm. We report the *Brillouin elastic contrast* to normalize the numerical values between experiments and wavelengths. The use of a dimensionless quantity $\overline{\nu}_B$ was proposed by Antonacci *et al.* [31] where

$$\overline{\nu}_B = \nu_B / \nu_B^{(W)} - 1 \quad (1)$$

such that ν_B is the measured Brillouin frequency shift of the sample and $\nu_B^{(W)}$ is the Brillouin frequency shift of distilled water.

D. Statistical Analysis

For the flow experiments, a paired t-test assuming equal variances was used to compare to the non-treatment group. For medium exchange and nutrient experiments, a one-way ANOVA was used to compare groups. All statistics were performed using GraphPad Prism7. *≤ 0.05 ** ≤ 0.01, *** ≤ 0.001, **** ≤ 0.0001.

III. Results and Discussion

A. Nodules decrease Brillouin shift under flow

To probe the cellular-mechanical effects of flow, we utilized Brillouin confocal microscopy, which enables access to tumors in a perfusion chamber without direct contact. Measurements were acquired following 7 days of continuous perfusion of medium. As a control, tumors nodules were seeded onto Matrigel in static cultures using a 24-well plate. Three independent experiments were performed with a total of n = 26 static nodules and n= 27 flow nodules. Brillouin maps were acquired along the XZ axis with 2 µm step size in both dimensions. **Fig. 2(a)** shows three representative Brillouin images from the three independent experiments. As shown in **Fig. 2(b),** nodules in the static condition had an average Brillouin shift (532 nm) of 7.92 ± 0.02 GHz (0.062 ± 0.003 Brillouin elastic contrast) while the tumors under flow had an average Brillouin shift (532 nm) of 7.85 ± 0.02 GHz (0.052 ± 0.003 Brillouin elastic contrast).

We used an empirical correlation between longitudinal and Young's modulus previously obtained on nodules to estimate the corresponding Young's modulus [27]. Longitudinal modulus (M') is defined as

$$M' = \frac{\rho \lambda^2 \Omega^2}{4n^2} \quad (2)$$

where ρ is the mass density, λ is the optical wavelength, Ω is the Brillouin shift, and n is the refractive index. We estimated the refractive index to be 1.37 and density is 1.08 kg/m^3, similar to that of single cells [26]. This equates to a longitudinal modulus of 2.55 MPa for static nodules and 2.51 for flow nodules, corresponding to approximately a 13% decrease in Young's modulus.

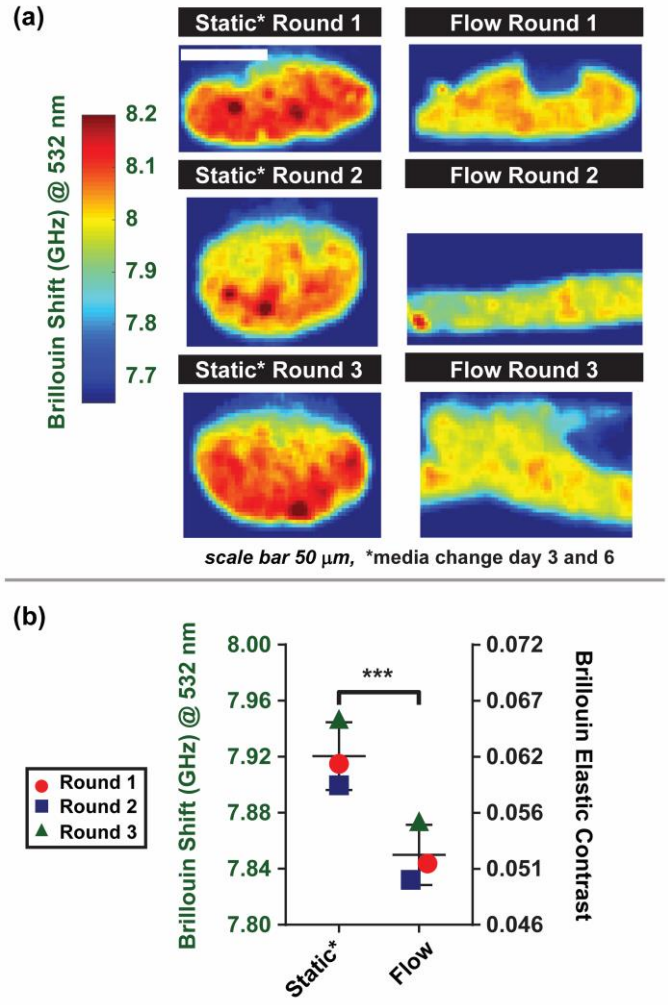

Fig. 2. (a) Representative Brillouin paired images from 3 independent experiments. Brillouin images were acquired in the XZ plane perpendicular to the stage. The color bar scale indicates the Brillouin shift in GHz where an increase in number (warmer color) indicates a stiffer material. The scale bar is 50 μm. (b) (Left axis) Comparison of static and flow conditions for 3 individual rounds. Brillouin shifts were acquired using a 532 nm laser. A paired t-test was used to show significant reduction ($p \leq 0.001$) of the Brillouin shift under flow. (Right axis) Conversion of Brillouin shift to Brillouin elastic contrast.

B. Effects of frequency of medium change on osmolality and growth of tumor nodules

To explain differences in Brillouin shift between flow and static, we proposed the fluid osmolality of medium could influence mechanics. We first evaluated the osmolality of medium with varying renewal frequencies: no medium change (red squares), medium change on days 3 and 6 (black circles), and daily medium change for 7 days (green triangles) (**Fig. 3**).

No medium change caused a significant rise ($p \leq 0.0001$) in osmolality (mOsm/kg H_2O) compared to the daily medium change and medium change on days 3/6. The control PBS (blue diamonds) shows the variability of the osmometer system (292 ± 3 mOsm/kg H_2O). As expected, in static cultures if the medium is not replenished, waste builds up causing a rise in solute particles inside the well. Another apparent effect of medium change frequency was on tumor growth. As shown in Fig. 4(a), (b), nodules that experienced no medium change over a course of 7 days had significantly smaller nodule areas (μm^2) compared with nodules that either experienced medium changes on days 3/6 ($p \leq 0.01$) or daily ($p \leq 0.0001$).

C. Brillouin shift corresponds to medium osmolality, but not cumulatively

Given that medium change frequency influences osmolality, we sought to determine the role of osmolality on mechanics. On day 7, Brillouin maps of tumor nodules were acquired in the XZ plane using 1 μm step size (**Fig. 5(a)**). Nodules with no medium change for 7 days had an average Brillouin shift of 6.42 ± 0.01 GHz (0.068 ± 0.001 Brillouin elastic contrast) while nodules with daily medium changes had a significantly lower Brillouin shift of 6.36 GHz ± 0.02 GHz (0.058 ± 0.003 Brillouin elastic contrast) ($p \leq 0.0001$).

We next asked if there was a cumulative effect of osmolality changes on the Brillouin shift. Here, we tested whether changing the medium on day 7 of the no medium change group would maintain an increased Brillouin shift, or regress to the daily medium change condition. Interestingly, we found that these nodules reduced their Brillouin shift immediately after the medium was changed. The average Brillouin shift after the medium change on day 7 was 6.37 ± 0.01 GHz (0.060 ± 0.002

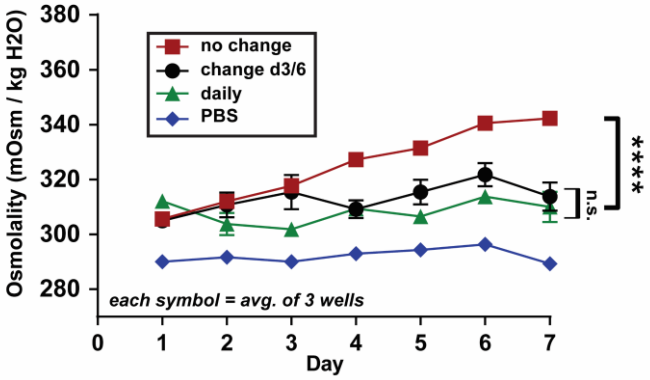

Fig. 3. Osmolality of medium over time. No medium change (red squares) resulted in a significant rise in osmolality compared to medium changes on days 3/6 (black circles) and daily medium changes (green triangles).

Brillion Elastic Contrast), which was not significantly different compared to the daily medium change condition (**Fig. 5(b),(c)**).

Altogether, these results demonstrated that osmolality influences tumor mechanics with short-time scales. The lack of a cumulative effect of osmolality on the Brillouin shift supports the idea that the differences observed between flow and static conditions in **Fig. 2** are minimally affected by osmolality since the osmotic states were matched on day 7 (**Fig. 3**).

D. Nutrient supply does not affect the Brillouin shift

In our previous experiment, we varied the frequency of medium changes; however, there was also a variation of the level of nutrients supplied. For example, changing the medium every day provided ~700 μl of FBS total compared to no medium changes, which provided ~100 μl of FBS total. Thus, we asked whether differences in the availability of nutrients have a direct effect on the mechanical properties of tumors. To

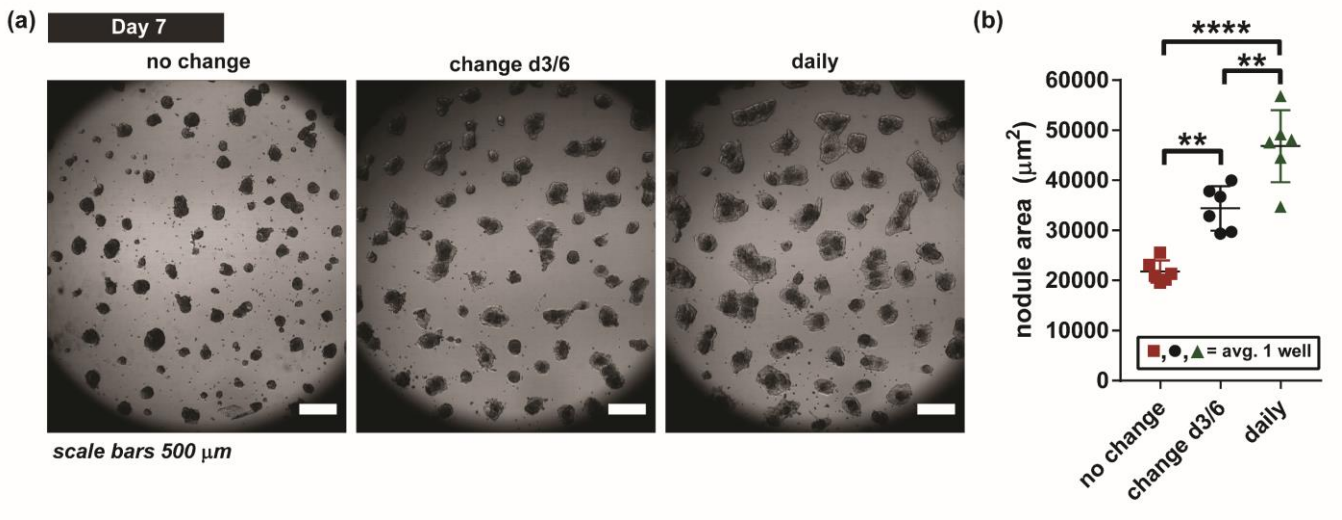

Fig. 4 (a) Brightfield images of adherent ovarian cancer nodules in static cultures on day 7 for three experimental conditions: no medium change (left panel), medium changes on days 3/6 (middle panel), and daily medium changes (right panel). Scale bars = 500 μm. (b) Nodule area on day 7 for the three medium change conditions shown in (a). There were significant differences in nodule area between no medium change (red squares), medium changes on days 3/6 (black circles), and the daily medium change (green triangles) conditions ($p \leq 0.0001$).

test this, nodules were cultured for 7 days in 1mL of medium supplemented with 0.1%, 1%, and 10% FBS. As expected, higher levels of nutrients caused more growth as pictured in **Fig. 6(a)**. On day 3, we measured the Brillouin shift of 9 nodules per 0.1% FBS and 10% FBS conditions and found no significant differences between the groups (**Fig. 6(b)**). Similarly, we measured the osmolality of the medium and found no significant differences (**Fig. 6(c)**). Our findings demonstrate that changes in nutrients have a negligible effect on tumor mechanical properties, compared to osmolality, which has a strong effect (**Figs. 3-5**). In addition, the growth of nodules in these altered FBS concentration conditions appears to be independent of Brillouin shift.

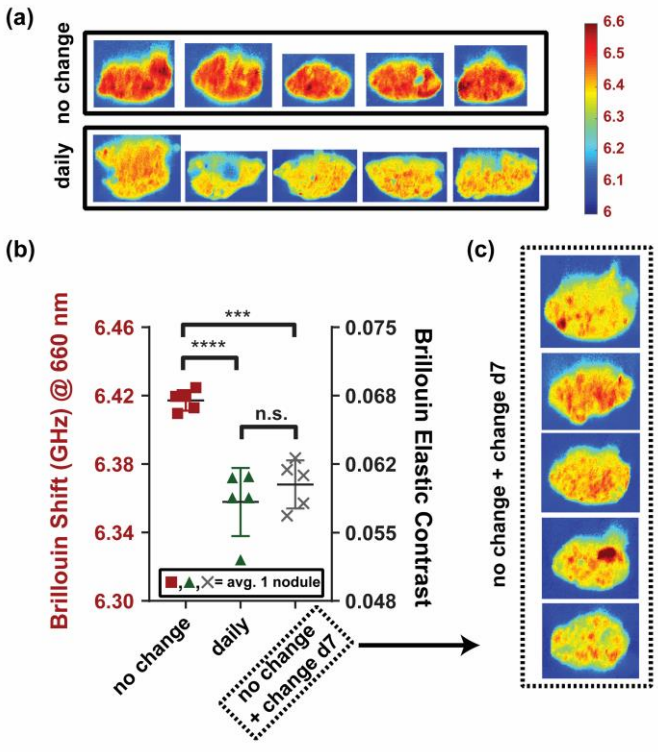

Fig. 5. Brillouin maps are pictured of nodules grown with no medium changes (top row) and with daily medium changes (bottom row). Images were acquired in the XZ plane, perpendicular to the Matrigel. (b) (Left Axis) The average Brillouin shift in the no medium change group (red squares) was significantly greater than the average Brillouin shift in the daily medium change group (green triangles) ($p \leq 0.0001$). A comparison of Brillouin shift in daily medium change and no medium change nodules for which medium was replenished on day 7 (grey X's) resulted in no significant differences, demonstrating a close relationship between osmolality of the culture medium and mechanical properties of the nodule. (Right axis) Conversion of Brillouin shift to Brillouin elastic contrast (c) Brillouin maps corresponding to the no medium change + change on day 7 condition.

IV. Conclusion

Here, we present the application of Brillouin confocal microscopy to investigate the mechanical properties of adherent ovarian cancer nodules grown in a perfusion chamber and subjected to flow for 7 days. It was found that flow caused a decrease in Brillouin shift (*i.e.* softening of the tumor nodule). We then performed a series of experiments to test other variables implicated in the flow and static conditions. In addition to shear stress, tumors under flow experienced a cumulatively lower osmolality and higher nutrient supply compared to the static control where medium was replaced on day 3 and 6. To examine the contribution of osmolality on Brillouin shift, we altered the frequency of medium changes in static nodules and found that higher fluid osmolality directly corresponded to an increased Brillouin shift. The lowest Brillouin shift was observed in the daily medium change condition, which had a Brillouin elastic contrast of 0.058 ± 0.003. However, we saw that having a cumulative osmolality difference, or history of higher osmolality did not affect mechanics. This was demonstrated by changing the medium on day 7 of nodules where medium was previously not

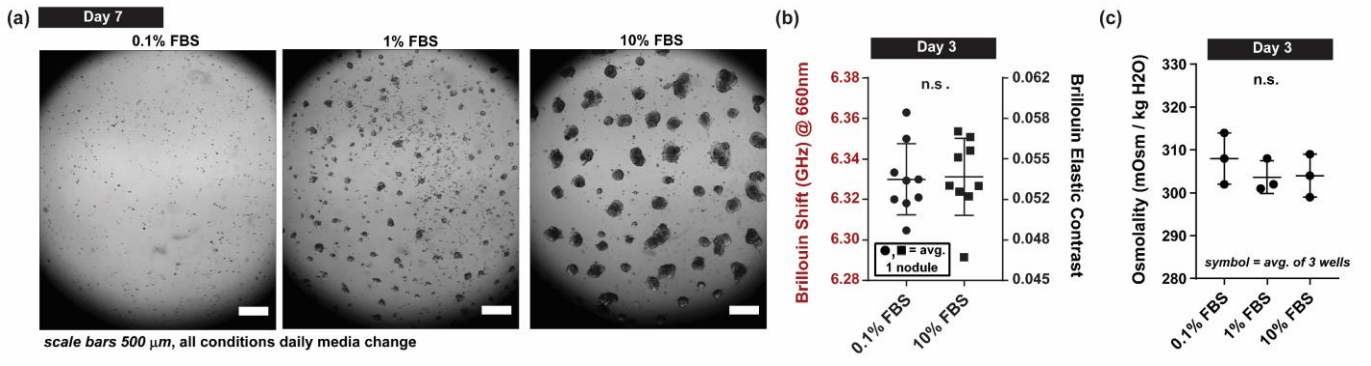

Fig. 6 (a) Nodules on day 7 cultured in 0.1%, 1%, and 10% FBS conditions. Scale bars are 500 μm. (b) (Left axis) Brillouin shift of nodules on culture day 3 revealed no significant differences between nodules grown in 0.1% FBS and 10% FBS medium. 9 nodules total for each condition were acquired in 3 separate wells. (Right axis) Conversion of Brillouin shift to Brillouin elastic contrast. (c) Osmolality of 0.1% FBS, 1% FBS, and 10% FBS culture medium incubated for 3 days in tumor cultures had no significant difference.

replenished. The Brillouin elastic contrast of no medium change + change day 7 had a Brillouin elastic contrast of 0.060 ± 0.002, which was not significantly different from the daily medium change group. Combined with the evidence that nodules under flow showed a significant decreased Brillouin elastic contrast (0.052 ± 0.003) compared to the daily medium change condition, and that the change day 3/6 medium osmolality is not significantly different from the daily medium osmolality (**Fig. 3**), we suspected osmotic influences were negligible in our flow versus static experiments. Finally, we showed that while higher FBS supplementation enhanced nodule growth, there were no effects on mechanical properties. Altogether, we attribute the observed decrease in Brillouin shift under flow to shear stress effects, with minimal contributions due to osmolality differences. Nonetheless, we emphasize the importance of considering osmolality differences during experimental designs.

The potency of a cell's perception to a variety of microenvironmental mechanical forces such as fluid shear stress, osmolality, and ECM solid stresses remains unknown. Likely, cells sense multiple cues which can compete or synergize to influence a cell's action [32]. Combined with previous works which analyze the molecular effects of tumor nodules under flow, there appears to be a relationship between decreased tumor stiffness and activation of EGFR and EMT signaling events. Yet, understanding the correlation between mechanics and biochemical signaling requires a deeper investigation. The fact that fluid shear stress promotes cytoskeletal rearrangement and differential expression of junctional molecules is consistent with observations of the effects of fluid shear stress on vascular endothelial cells [33]–[35]. While the upstream flow sensing molecules and mechanisms remain unknown, cytoskeletal remodeling is accompanied by changes in cell stiffness in endothelial cells [35]–[37], suggesting that our observed changes in nodule stiffness could be related to cytoskeletal remodeling.

The strong relationship between water fraction and mechanical properties warrants a discussion on the contribution to mechanical properties by solid and fluid components within cells and other biological materials. Recently, Guo *et al.*, revealed a strong relationship between cell volume and mechanical properties independent of perturbation method in single cells (e.g. substrate stiffness, osmotic shock, cytoskeletal perturbation). Han *et al.* also demonstrated in tumors that cells at the periphery were both softer and larger [38]. Here, the strong relationship of medium osmolality and the Brillouin shift was substantiated when we found that the mechanical properties could be instantaneously reversed by changing the surrounding fluid osmolality.

Given Brillouin microscopy is an optical approach, this technology offers unique experimental advantages compared to traditional testing systems such as atomic force microscopy (AFM) which require contact with the sample. However, the longitudinal modulus probed by Brillouin scattering is not directly related to the Young's modulus measured by conventional methods. Indeed, the difference in frequency probed (GHz vs quasi-static) and the near incompressibility of biological materials make the two moduli vary by orders of magnitude in absolute values. Nevertheless, numerous experiments find strong correlations in biological samples, including cells, tissues and nodules [25]–[27], [39]. These studies establish an empirical log-log linear relationship to allow estimating the changes to elastic modulus based on changes in Brillouin-derived longitudinal modulus [25]–[27], [39]. This is because both moduli are similarly affected by underlying properties such as polymerization, polymer branching, liquid-solid fraction and network tension [25]–[27], [39]–[41]. In recent years, several papers have been dedicated to the topic, specifically in terms of dependence on water content. In highly (~95%) hydrated materials, Brillouin signatures are strongly affected by hydration and thus become an unreliable estimator of traditional mechanical properties [42], [43]; instead, in the regime of cells, tissues and nodules, where we expect the water content to be approximately 70%, it has been shown that Brillouin technology can be used to estimate traditional mechanical properties after proper calibration [44], [45].

Our study has several limitations which are important to discuss. First, results were evaluated using a single ovarian cancer cell line. Therefore, the effects observed here cannot be generalized until assessments on other ovarian cancer and non-cancerous cell lines are performed. Second, nodules are formed across multiple depths [11], [12], yet imaging was performed in one XZ plane; thus, any heterogeneity and directionality dependencies of flow on intratumoral mechanics was disregarded in our analysis. Third, the physiological relevance

of osmolality of the tumor microenvironment is largely unknown in the context of ovarian cancer. Particularly, there is a vital need to characterize the osmolality of ascites. Here, we use a perfusion model where fresh medium was supplied. Other groups suggest the use of a perfusion system with medium recirculation, which would inevitably trigger a higher osmolality over time. As gathered from our experiments and the work of others, understanding the contributions of osmolality and shear stress, among other physical factors such as substrate stiffness, are critical to appropriately model the clinical state. Therefore, careful consideration of these factors should be made in the design of future perfusion systems. Finally, here we test a single time-point (7 day) and shear stress (3 dyne/cm^2). Measuring at varying durations and rates could give insight to time and stress-dependencies on mechanics.

To conclude, this study analyzes the response of mechanical properties to flow by utilizing Brillouin confocal microscopy, an optical approach with uniquely enables access to confined tumors within a microfluidic chip. Previously, flow has been shown to alter cell morphology, protein/gene profile, and chemoresistance [11], [12], [21], [48]; here, we show flow also alters mechanical properties. Given this initial evidence of a link between mechanics and chemoresistant phenotype, altering cell mechanics could be considered as a therapeutic target in the future.

REFERENCES

[1] C. K. M. Ip *et al.*, "Stemness and chemoresistance in epithelial ovarian carcinoma cells under shear stress," *Sci. Rep.*, vol. 6, p. 26788, Jun. 2016.

[2] J. Shen-Gunther and R. S. Mannel, "Ascites as a Predictor of Ovarian Malignancy," *Gynecol. Oncol.*, vol. 87, no. 1, pp. 77–83, 2002.

[3] H. Huang *et al.*, "Clinical significance of ascites in epithelial ovarian cancer," *Neoplasma*, vol. 60, no. 5, pp. 546–552, 2013.

[4] I. Lai, M. N. Daniel, B. P. Rosen, T. May, C. Massey, and T. Feigenberg, "Correlation of differential ascites volume with primary cytoreductive surgery outcome, lymph node involvement, and disease recurrence in advanced ovarian cancer," *Int. J. Gynecol. Cancer*, vol. 29, no. 5, pp. 922 LP – 928, Jun. 2019.

[5] M. Stukan, "Drainage of malignant ascites: patient selection and perspectives," *Cancer Manag. Res.*, vol. 9, pp. 115–130, Apr. 2017.

[6] E. Kipps, D. S. P. Tan, and S. B. Kaye, "Meeting the challenge of ascites in ovarian cancer: new avenues for therapy and research," *Nat. Rev. Cancer*, vol. 13, no. 4, pp. 273–282, 2013.

[7] M.-F. Penet *et al.*, "Ascites Volumes and the Ovarian Cancer Microenvironment ," *Frontiers in Oncology* , vol. 8. p. 595, 2018.

[8] G. J. Ross, H. B. Kessler, M. R. Clair, R. A. Gatenby, W. H. Hartz, and L. V Ross, "Sonographically guided paracentesis for palliation of symptomatic malignant ascites," *Am. J. Roentgenol.*, vol. 153, no. 6, pp. 1309–1311, Dec. 1989.

[9] D. S. Tan, R. Agarwal, and S. B. Kaye, "Mechanisms of transcoelomic metastasis in ovarian cancer," *Lancet Oncol*, vol. 7, no. 11, pp. 925–934, 2006.

[10] B. K. Zebrowski, W. Liu, K. Ramirez, Y. Akagi, G. B. Mills, and L. M. Ellis, "Markedly Elevated Levels of Vascular Endothelial Growth Factor in Malignant Ascites," *Ann. Surg. Oncol.*, vol. 6, no. 4, p. 373, 1999.

[11] I. Rizvi *et al.*, "Flow induces epithelial-mesenchymal transition, cellular heterogeneity and biomarker modulation in 3D ovarian cancer nodules," *PNAS*, vol. 110, no. 22, pp. 1974–1983, 2013.

[12] I. Nath, Shubhankar; Pigula, Michael; Khan, Amjad P.; Hanna, William; Ruhi, Mustafa K.; Dehkordy, Farzaneh M.; Pushpavanam, Karthik; Rege, Kaushal; Moore, Kaitlin; Tsujita, Yujiro; Conrad, Christina; Inci, Fatih; del Carmen, Marcela G.; Franco, Walfre; Celli and S. P. Nath Michael; Khan, Amjad P.; Hanna, William; Ruhi, Mustafa K.; Dehkordy, Farzaneh M.; Pushpavanam, Karthik; Rege, Kaushal; Moore, Kaitlin; Tsujita, Yujiro; Conrad, Christina; Inci, Fatih; del Carmen, Marcela G.; Franco, Walfre; Celli, Imran., "Flow-induced Shear Stress Confers Resistance to Carboplatin in an Adherent Three-Dimensional Model for Ovarian Cancer: A Role for EGFR-Targeted Photoimmunotherapy Informed by Physical Stress," *J. Clin. Med.*, vol. 9, no. 4, p. 924, 2020.

[13] C. Novak, E. Horst, and G. Mehta, "Review: Mechanotransduction in ovarian cancer: Shearing into the unknown," *APL Bioeng.*, vol. 2, p. 31701, 2018.

[14] A. J. McKenzie, S. R. Hicks, K. V Svec, H. Naughton, Z. L. Edmunds, and A. K. Howe, "The mechanical microenvironment regulates ovarian cancer cell morphology, migration, and spheroid disaggregation," *Sci Rep*, vol. 8, no. 1, p. 7228, 2018.

[15] D. J. McGrail, Q. M. N. Kieu, and M. R. Dawson, "The malignancy of metastatic ovarian cancer cells is increased on soft matrices through a mechanosensitive Rho–ROCK pathway," *J Cell Sci*, vol. 127, pp. 2621–2626, 2014.

[16] W. Xu, R. Mezencev, B. Kim, L. Wang, J. McDonald, and T. Sulchek, "Cell Stiffness Is a Biomarker of the Metastatic Potential of Ovarian Cancer Cells," *PLoS One*, vol. 7, no. 10, p. e46609, 2012.

[17] A. N. Ketene, E. M. Schmelz, P. C. Roberts, and M. Agah, "The effects of cancer progression on the viscoelasticity of ovarian cell cytoskeleton structures," *Nanomedicine*, vol. 8, no. 3, pp. 93–102, 2012.

[18] V. Swaminathan, K. Mythreye, E. T. O'Brien, A. Berchuck, G. C. Blobe, and R. Superfine, "Mechanical stiffness grades metastatic potential in patient tumor cells and in cancer cell lines," *Cancer Res*, vol. 71, no. 15, pp. 5075–5080, 2011.

[19] C. Dong, X. Hu, and C. Z. Dinu, "Current status and perspectives in atomic force microscopy-based identification of cellular transformation," *Int J Nanomedicine*, vol. 11, pp. 2107–2118, 2016.

[20] A. Kapoor *et al.*, "Soft drug-resistant ovarian cancer cells migrate via two distinct mechanisms utilizing myosin II-based contractility," *Biochim. Biophys. Acta - Mol. Cell Res.*, vol. 1865, no. 2, pp. 392–405, 2018.

[21] L. Avraham-Chakim, D. Elad, U. Zaretsky, Y. Kloog, A. Jaffa, and D. Grisaru, "Fluid-flow induced wall shear stress and epithelial ovarian cancer peritoneal spreading," *PLoS One*, vol. 8, no. 4, pp. e60965–e60965, Apr. 2013.

[22] G. Scarcelli and S. H. Yun, "Confocal Brillouin microscopy for three-dimensional mechanical imaging," *Nat. Photonics*, vol. 2, no. 1, pp. 39–43, 2008.

[23] R. Prevedel, A. Diz-Muñoz, G. Ruocco, and G. Antonacci, "Brillouin microscopy: an emerging tool for mechanobiology," *Nat. Methods*, vol. 16, no. 10, pp. 969–977, 2019.

[24] G. Scarcelli, R. Pineda, and S. H. Yun, "Brillouin optical microscopy for corneal biomechanics," *Invest. Ophthalmol. Vis. Sci.*, vol. 53, no. 1, pp. 185–190, Jan. 2012.

[25] J. N. Webb, J. P. Su, and G. Scarcelli, "Mechanical outcome of accelerated corneal crosslinking evaluated by Brillouin microscopy," *J Cataract Refract Surg*, vol. 43, no. 11, pp. 1458–1463, 2017.

[26] G. Scarcelli *et al.*, "Noncontact three-dimensional mapping of intracellular hydro-mechanical properties by Brillouin microscopy," *Nat Methods*, vol. 12, no. 12, pp. 1132–1134, 2015.

[27] C. Conrad, K. M. Gray, K. M. Stroka, I. Rizvi, and G. Scarcelli, "Mechanical Characterization of 3D Ovarian Cancer Nodules Using Brillouin Confocal Microscopy," *Cell. Mol. Bioeng.*, 2019.

[28] B. Jeffrey, H. S. Udaykumar, and K. S. Schulze, "Flow fields generated by peristaltic reflex in isolated guinea pig ileum: impact of contraction depth and shoulders," *Am. J. Physiol. Liver Physiol.*, vol. 285, no. 5, pp. G907–G918, Nov. 2003.

[29] J. Schindelin *et al.*, "Fiji: an open-source platform for biological-image analysis," *Nat. Methods*, vol. 9, p. 676, 2012.

[30] M. Nikolić and G. Scarcelli, "Long-term Brillouin imaging of live cells with reduced absorption-mediated damage at 660 nm wavelength," *Biomed. Opt. Express*, vol. 10, no. 4, pp. 1567–1580, Mar. 2019.

[31] G. Antonacci *et al.*, "Recent progress and current opinions in Brillouin microscopy for life science applications," *Biophys. Rev.*, vol. 12, no. 3, pp. 615–624, Jun. 2020.

[32] A. J. Keung, S. Kumar, and D. V Schaffer, "Presentation counts: microenvironmental regulation of stem cells by biophysical and material cues," *Annu. Rev. Cell Dev. Biol.*, vol. 26, pp. 533–556, 2010.

[33] W. J. Polacheck *et al.*, "A non-canonical Notch complex regulates adherens junctions and vascular barrier function," *Nature*, vol. 552, p. 258, 2017.

[34] E. Tzima *et al.*, "A Mechanosensory Complex That Mediates the Endothelial Cell Response to Fluid Shear Stress," *Nature*, vol. 437, pp. 426–431, Oct. 2005.

[35] J. H. Dangaria and P. J. Butler, "Macrorheology and adaptive microrheology of endothelial cells subjected to fluid shear stress," *Am. J. Physiol. Cell Physiol.*, vol. 293, no. 5, pp. C1568–C1575, Nov. 2007.

[36] F. T. Arce *et al.*, "Regulation of the Micromechanical Properties of Pulmonary Endothelium by S1P and Thrombin: Role of Cortactin," *Biophys. J.*, vol. 95, no. 2, pp. 886–894, 2008.

[37] J. Fels, P. Jeggle, I. Liashkovich, W. Peters, and H. Oberleithner, "Nanomechanics of vascular endothelium," *Cell Tissue Res.*, vol. 355, no. 3, pp. 727–737, 2014.

[38] Y. L. Han *et al.*, "Cell swelling, softening and invasion in a three-dimensional breast cancer model," *Nat. Phys.*, 2019.

[39] G. Scarcelli, P. Kim, and S. H. Yun, "In vivo measurement of age-related stiffening in the crystalline lens by Brillouin optical microscopy," *Biophys J*, vol. 101, no. 6, pp. 1539–1545, 2011.

[40] M. Guo *et al.*, "Cell volume change through water efflux impacts cell stiffness and stem cell fate," *PNAS*, vol. 114, no. 41, pp. E8618-e8627, 2017.

[41] M. L. Gardel, J. H. Shin, F. C. MacKintosh, L. Mahadevan, P. Matsudaira, and D. A. Weitz, "Elastic Behavior of Cross-Linked and Bundled Actin Networks," *Science (80-.).*, vol. 304, no. 5675, pp. 1301 LP – 1305, May 2004.

[42] G. Scarcelli and S. H. Yun, "Reply to 'Water content, not stifness, dominates Brillouin spectroscopy measurements in hydrated materials,'" *Nat. Methods*, vol. 15, pp. 561–565, 2018.

[43] P.-J. Wu *et al.*, "Water content, not stiffness, dominates Brillouin spectroscopy measurements in hydrated materials," *Nat. Methods*, vol. 15, no. 8, p. 561, 2018.

[44] P. Shao *et al.*, "Effects of Corneal Hydration on Brillouin Microscopy in Vivo," *Invest. Ophthalmol. Vis. Sci.*, vol. 59, pp. 3020–3027, 2018.

[45] J. Webb, H. Zhang, A. Sinha Roy, J. Randleman, and G. Scarcelli, "Detecting Mechanical Anisotropy of the Cornea Using Brillouin Microscopy," *Transl. Vis. Sci. Technol.*, vol. in press, 2020.

[46] J. Frede *et al.*, "Ovarian cancer: Ion channel and aquaporin expression as novel targets of clinical potential," *Eur. J. Cancer*, vol. 49, no. 10, pp. 2331–2344, 2013.

[47] V. K. Sidhaye, K. S. Schweitzer, M. J. Caterina, L. Shimoda, and L. S. King, "Shear stress regulates aquaporin-5 and airway epithelial barrier function," *Proc. Natl. Acad. Sci.*, vol. 105, no. 9, pp. 3345 LP – 3350, Mar. 2008.

[48] A. R. Hyler *et al.*, "Fluid shear stress impacts ovarian cancer cell viability, subcellular organization, and promotes genomic instability," *PLoS One*, vol. 13, no. 3, p. e0194170, 2018.